Fuel 301 (2021) 121029

Contents lists available at ScienceDirect

Fuel

journal homepage: www.elsevier.com/locate/fuel

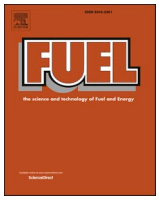

Full Length Article

Nox emissions reduction analysis in a diesel Euro VI Heavy Duty vehicle using a thermoelectric generator and an exhaust heater

J. Ximinis, A. Massaguer, T. Pujol, E. Massaguer *

Department of Mechanical Engineering and Industrial Construction, University of Girona, C. Universitat de Girona, 4, 17003 Girona, Spain

ARTICLE INFO

Keywords:
Thermoelectric generator
Catalyst efficiency
NOx reduction
Heavy Duty vehicle
SCR efficiency
ATEG

ABSTRACT

Selective Catalytic Reduction systems (SCR) are very efficient on reducing NOx. However, they only perform properly when exhaust gas temperature is higher than 180 °C. This means that for low engine regimes combined with cold engine temperatures, SCR systems remains inactive.

This study presents a new approach to minimize the amount of NOx emitted by diesel engines of Heavy-Duty Vehicles during low engine regimes and low exhaust gases temperature conditions. We propose the addition of an Automotive Thermoelectric Generator (ATEG) coupled to an electric Exhaust Gas Heater (EGH) to make the SCR system inject the urea solution at low engine regimes. This EGH-ATEG system, which can be retrofitted in any existing vehicle, is designed to be energetically closed, so there is no extra consumption of fuel. Experimental results show that NOx emissions can be reduced up to 80% when an EGH is added to a standard diesel-powered Euro VI Heavy Duty truck configuration. Apart from that, the use of an ATEG installed downstream of the aftertreatment system can produce the energy required by the EGH, which means that the EGH-ATEG system can work energetically autonomous and independent from the vehicle's electrical system. This system can improve SCR efficiency up to 55% during low engine regimes.

1. Introduction

A large proportion of buses and trucks operating in the EU's urban areas are still diesel-powered. In addition, many of them are not yet close to the end of their life [1]. They suffer from generation of gas pollutants, particularly oxides of nitrogen (NOx) [2], which are facing increasingly severe emission regulations.

However, these vehicles may be retrofitted with efficient exhaust aftertreatment devices.

Several systems allow high NOx reduction such as EGR (Exhaust Gas Recirculation), NOx absorbers, lean NOx catalyst systems and SCRs (Selective Catalytic Reduction).

NOx absorbers have a high operating temperature window, being highly sensitive to sulphur poisoning. On the other hand, lean NOx catalyst systems are not suitable for mobile vehicles due to their poor thermal conductivity and narrow temperature window. EGRs are used nowadays in vehicles after demonstrating to be a reliable and effective system. NOx emission can be reduced by 50% in absolute numbers using this technology. SCR systems compared with technologies mentioned before, achieve more than 90% of NOx emissions reduction [3].

SCR works as an advanced active emissions control that converts nitrogen oxides (NOx) into diatomic nitrogen (N_2) and water (H_2O) with the aid of a catalyst. A reducing agent, a solution of urea (32.5%) and distilled water commonly known as AdBlue, is needed to achieve this conversion reaction. This urea solution is decomposed into water vapor and ammonia that is adsorbed on the catalyst substrate as it is injected before SCR. Finally, adsorbed ammonia reacts with NOx and is reduced into harmless water vapor and nitrogen.

Concerning urea solution evaporative process, some studies report that catalyst reaction is mainly affected by temperature and the spatial droplet size [4]. Different operating conditions and modified solution injector designs can cause a variation in the reaction rate of this process. Recent researches have remarked that this process strongly depends on temperature [5,6]. Ammonia process reaction generally starts from 180 °C, reaching its maximum reaction rate around 350 °C [7]. When exhaust gas temperature is lower than 180 °C, urea decomposition reaction can generate derivatives such as cyanuric acid, biuret, melamine, ammelide and ammeline as deposits on pipe wall [8], which are highly undesired for impeding the regular flow of gases. In order to avoid by-products, urea injection generally starts when exhaust gas temperature

* Corresponding author at: Department of Mechanical Engineering and Industrial Construction, University of Girona, C. Universitat de Girona, 4, 17003 Girona, Spain.

https://doi.org/10.1016/j.fuel.2021.121029
Received 28 December 2020; Received in revised form 21 April 2021; Accepted 8 May 2021

is higher than 180 °C.

Fig. 1 is a static map of SCR efficiency. In order to achieve maximum de-NOx efficiency (around 0.95) the catalyst requires temperatures over 230 °C. This paper is focused on the first step of this heating process, reducing the time to achieve the proper target temperature when the urea solution is injected into the conversion system. This low temperature range (up to 130 °C) can be found at engine starts, during inter-urban routes or in vehicle operation modes with minor engine loads. SCR efficiency is also affected by ammonia storage and injection control of urea solution, both out of our scope.

Heavy Duty Vehicles (HDVs) for local freight transport, municipal vehicles and delivery vans are often driven for only short distances or through frequently interrupted routes. Under these driving conditions, these engines may not achieve the minimum exhaust gas temperature required to cut nitrogen oxide emissions effectively with conventional SCR systems. Gao et al. [10] demonstrated that more than 50% of exhaust gas emissions, in a given driving cycle, are emitted during cold starts.

Hybrid Electrical Vehicles (HEVs) also face the challenge of high NOx emissions, as its internal combustion engine are commonly switched off at low speed and wheel torque, when the brake specific fuel consumption is especially high. Hybrid diesel buses present higher NOx values compared to full diesel buses. The poor SCR efficiency in HEVs is a consequence of low exhaust gas temperatures [11,12]. Recent studies demonstrated that NOx emissions can increase around 30% for hybrid powertrains in urban real-life cycles [13]. Therefore, the thermal management of the catalyst is fundamental for both HEVs and conventional vehicles.

In this regard, many strategies have been applied to develop highly efficient low temperature catalysts [14,15]. However, these catalytic materials present some drawbacks such as catalyst poisoning by H_2O or/ and SO_2. Hence, active investigation is being held in order to achieve a suitable NOx conversion without compromising feasibility for this SCR catalysts [16].

Avoiding heat leakage of exhaust gases is another strategy to mitigate the low temperature problem. A double-wall insulation system can be mounted over the exhaust pipe between the urea solution injector and the SCR element [17]. However, this method only represents a 0.6% improvement of SCR efficiency.

Jiang et al. [18] and Hamedi et al. [19] proposed the use of a Phase Change Material (PCM) in order to store excess thermal energy from exhaust gases. This energy can be released in a controllable way in order to maintain relatively stable exhaust gas temperatures. The systems proposed combine exhaust gas temperature control and an SCR that can improve NOx emission conversion up to 38%.

Finally, some active heating systems have been developed to shorten the time in which the SCR unit is not operative.

Okada et al. [20] suggested a method that consists in directly heating the urea using glow plugs as heat source. In this research, they considered improving the ammonia generation efficiency by urea reforming. This system allowed to achieve a 60% conversion of NOx at 160 °C on a conventional SCR system. The system was able to generate ammonia with an efficiency of more than 90%.

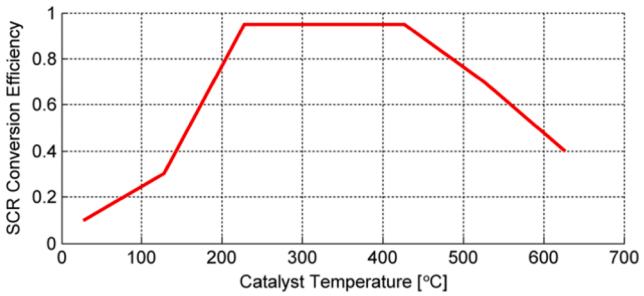

Fig. 1. SCR conversion efficiency as a function of catalyst temperature [9].

Rink et al. developed a catalytic converter that incorporate an internal electrical resistance for preheating the catalyst have been tested with relevant results [21,22].

Sharp et al. [23] compared several options to achieve ultra-low NOx emissions on a 361 kW Volvo MD13TC engine with a fixed geometry turbocharger. Among others, a 2 kW electrically heated catalyst, followed by a hydrolysis catalyst alone or in combination with a 5 kW additional heater placed downstream the DPF and before the DEF injection point, was investigated and compared to an adjustable-power mini-burner going from 8 kW to20 kW. These systems can bring, respectively, a 45%, 70%, and 80% potential reduction in the overall tailpipe NOx emissions at the expense of increased energy consumption that has to be carefully quantified.

Culbertson et al. [24] studied the ability of an electric heater to effectively raise the temperature of the exhaust and overcome the effect of moisture and low exhaust temperature, allowing NOx conversion to begin sooner. Different electric heaters from 12 kW to 30 kW was used to heat the exhaust gases of a Cummins ISDe 6.7 L engine. Results shown that it is possible to achieve high NOx conversion temperatures quickly with robust heater technology that is suited for diesel applications.

However, the energy consumed by electrical heaters tested in these studies assumed that they were powered by the vehicle's electrical system. Therefore, to proceed to an overall evaluation, the impact of such systems on fuel consumption and overall vehicle efficiency must be addressed.

Recently, a theoretical study [25] demonstrates that the use of an Exhaust Gas Heater (EGH) coupled to an Automotive Thermoelectric Generator (ATEG) can improve the aftertreatment's efficiency of a light-duty vehicle (LDV) in cold-starts without the need of using extra energy. On one hand the EGH is used to raise exhaust temperatures before the catalyst. On the other side, the ATEG is used to convert waste exhaust heat, downstream of the aftertreatment system, into electricity. This energy is stored into a specific battery, which is used lately by the EGH when exhaust gases are cold.

On the basis of [25], the main objective of this study is to experimentally demonstrate that this system, an EGH-ATEG, can work energetically closed and can reduce NOx emissions in diesel-powered HDVs during low demanding regimes. Unlike [25], in this study the EGH is used to heat the exhaust gases upstream of the SCR during low-speed regimes. This will shorten the time required to reach the SCR light-off temperature where AdBlue is injected and will improve NOx emissions reduction. Additionally, a secondary objective is proposed: demonstrate that this system can work energetically autonomous and independent from the vehicle's electrical system.

To carry out this study, (i) an EGH has been installed to the most suitable position of the exhaust gas system, before the aftertreatment unit. The EGH behaviour has been tested experimentally under steady state driving conditions using a MAN TGX EURO VI on a dynamometer roller bench. (ii) The gathered information from the experiments has been used to analyse the viability of the proposed EGH under different heating power set points. Furthermore, (iii) the obtained data is introduced in a theoretical ATEG simulation software to prove its viability as an exclusive power source for the EGH during low engine regimes.

2. EGH-ATEG system

As stated before, the proposed system to reduce NOx emissions consists in a combination of the standard vehicle parts and specific added components such as an EGH. In this first approach, we will focus particularly on each part assembled downstream the exhaust pipe. There is a detailed description for the standard components of the HDV tested in Section 3. This system is designed to work in two different stages illustrated in Fig. 2.

Heating stage (1): this first step consists in rising the exhaust gas temperatures using the EGH. This device, an electrical resistance,

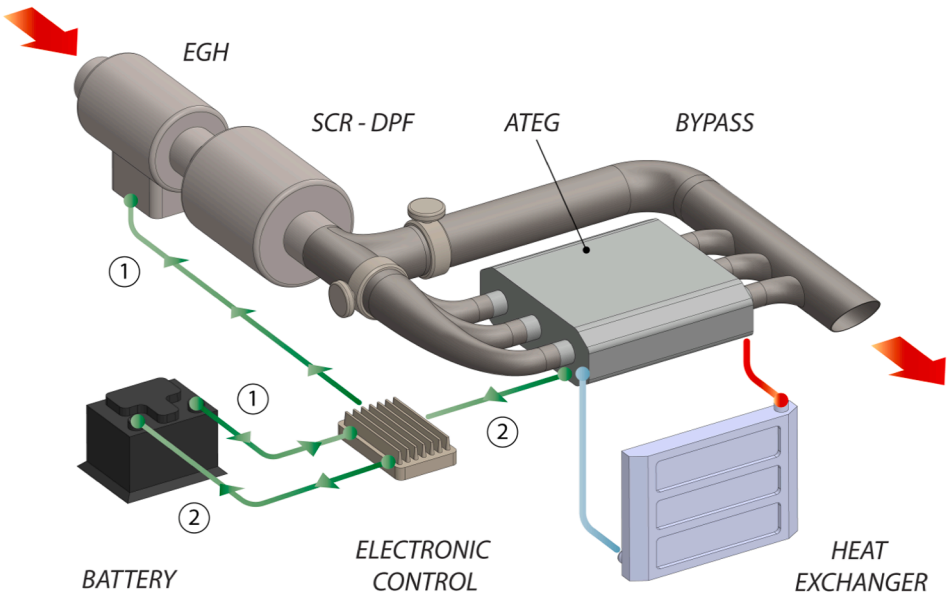

Fig. 2. Proposed EGH-ATEG solution with the electrical energy flows: heating stage (1) and recovery stage (2).

consumes power from a dedicated electrical battery. The goal of this phase is to increase the exhaust gas temperature at SCR inlet. The beginning of this stage is when the engine starts as exhaust gases are on its lowest temperature level. The duration of this stage is determined by the target temperature (=180 °C), being around 12 min at idling in this tested vehicle using its standard exhaust system. Reaching this target temperature (=180 °C) is crucial because at this point urea solution is dosed into the system and its catalyst reaction is made properly, obtaining a faster and more efficient NOx reduction.

Recovery stage (2): this second step is related to ATEG conversion of thermal energy from exhaust gases into electricity. This electrical power is managed by the electronic control that stores it into the dedicated battery. This step starts when the engine is turned on and it can last up to 240 min (by assuming a maximum continuous driving time limited to 4 h). The objective of this second phase is to maximize the amount of electrical energy stored for its later use by the EGH under low engine regime conditions. Note that the power generated by the ATEG (P_{ATEG}) increase with the engine regime [26,27]. At high engine regimes, exhaust temperatures are higher, increasing the temperature difference between the hot side and the cold side of each thermoelectric module (TEM), $\Delta T = T_{HOT} - T_{COLD}$. Considering that $P_{ATEG} \propto \Delta T^2$, it can be concluded that the higher the engine regime, the higher the power generated by the ATEG. Moreover, the longer the time spend at high engine regimes (e.g. greater than 80 km/h), the higher the energy recovered by the ATEG. Therefore, long-distance transport vehicles are the most suitable to incorporate the TATH.

Regarding the exhaust gas flow, each component of the proposed system is specifically located in order to optimize its functionality. If we begin upstream the aftertreatment system, and after the turbocharger, we find the EGH. This component is located just before the standard SCR and DPF (Diesel Particle Filter) package of the vehicle. This standard lot of components includes the urea dosing system, not represented in Fig. 2, and they are explained in the following section. The specific location of the EGH is important as it will maximize its impact into the standard NOx reduction system by providing a rise in temperature with minimal thermal loss. On the outlet side of the standard SCR-DPF package there is a bypass represented by a bifurcation of the exhaust pipe. Its function is to avoid high exhaust gas temperatures that damage the ATEG thermoelectric modules. Fig. 2 represents an external solution that uses electrical valves to modulate the gas flow. However, Massaguer et al. have also developed an internal solution proven to succeed in its aim [25]. The ATEG is located at the end of the exhaust system. It is important to be downstream of SCR as ATEG reduces the temperature of the exhaust gases and SCR needs a high temperature in order to perform efficiently. Furthermore, ATEG thermal loss will be reduced as post SCR catalytic converters rise exhaust gas temperature when performing.

The objective of obtaining emissions reduction without adding extra fuel consumption requires a compromise between energy consumed and produced. This system operates in two stages, as explained before. Heating stage (1) and recovery stage (2) are represented in Fig. 2 by its energy flow respectively. In the first stage, the control unit feeds the EGHh with the energy stored in the battery. In the second stage, the control unit feeds the battery with the energy recovered by the ATEG. ATEG requires a cold focus, then the thermal scheme is complemented with a cooling circuit composed by a low temperature heat exchanger and a water pump (not represented in Fig. 2)

Note that the inclusion of the EGH and the ATEG may cause a backpressure (BP) increase in the exhaust pipe. Massaguer et al. [26,27] analysed this effect in a light duty vehicle (engine power < 100 kW) and demonstrated that if the BP increase stays below 40 mbar, the vehicle's fuel consumption is not affected. In [28], authors tested an ATEG in a light-duty vehicle with a maximum power production of 200 W, a weight of 8 kg and a maximum backpressure of 10 mbar. They observed that the BP caused in the exhaust pipe did not adversely affect engine performance. A part form that, according to the fuel economy assessment method of ref. [27], the additional weight of the ATEG (i.e. generator and cooling system) only suppose an increase of 0.08% in fuel consumption. Considering that the ATEG used in this study is based on the model developed in [28], both the backpressure and the additional weight added by the ATEG has been neglected.

Finally, the EGH was tested in a hot air flow bank under the maximum exhaust conditions: 1700 rpm and 358 kW to analyse its backpressure. The results from this test showed a maximum pressure loss of 1.8 mbar at 416 g/s. With this information it can be concluded that the inclusion of the EGH into the exhaust system will not adversely affect the engine performance.

3. Experimental set up

The active and most demanding antipollution standard for HDV in the European Union is the Euro VI standard (Euro VII is planned for fourth quarter 2021). This current regulation is a great challenge,

especially for Heavy Duty Vehicle manufacturers. The most common system adopted for manufacturers consists on the combination of sophisticated ECU (Engine Control Unit) software, together with a catalytic chemical reaction, to obtain NOx ppm values below antipollution regulation limits. In this study, a Heavy-Duty Vehicle Euro VI TGX 18.480 Efficient Line 2 from MAN is used to carry out the tests. Fig. 3 shows this vehicle disposition and the main data acquisition that include the ECU and the rolling bench controls.

The system used consisted of an EGH located upstream of the standard aftertreatment system, see Fig. 4. The EGH is a Watlow ECOTEG unit with 12 kW of power. This device contains an electric heating coil controlled by a temperature regulation system designed specifically for this application. In order to simplify the test, a three-phase circuit externally powered the EGH. The regulation was done through a specific control unit that adjusted the power injected to the EGH according to the temperature set point. A discussion about which are the most suitable heating power values according to the vehicle's electric capacity will be presented in Section 5. The whole system was laid out as seen in Fig. 5. Selected key parameters such as temperatures, ppm NOx or engine regime, are synchronized, monitored, and registered to guarantee future correlations while the heater was in use along all the tests.

In second place of exhaust gases circuit, we find a unit composed by a Diesel Oxidation Catalyst (DOC) and a DPF. The first one is in charge of oxidation of carbon monoxide (CO) and unburned hydrocarbons (HC). In addition, it allows a continuous regeneration of the DPF. This second one is very important to capture as many organic fraction (OF) of diesel particles as possible. Soot is the main component trapped in the filter walls, being burned when the DPF reaches a maximum backpressure. The manufacturer fixes this threshold value and when reached, a forced regeneration starts by injecting more fuel to rise exhaust gases temperature and burn the particles.

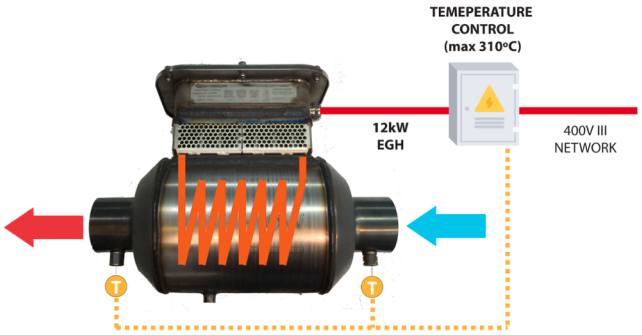

Fig. 4. Function scheme of the used EGH.

Downwards, we find a set of devices related to Diesel Exhaust Fluid (DEF) composed by the tank, the supply module and the dosing module. This particular vehicle uses a commercial urea solution as fluid, all this set is controlled by ECU parameters and this solution is not injected into the system until the exhaust gases reach 180 °C. The dosing module uses temperature and NOx sensors (one located before the DOC and another after the SCR) to adjust in real time the exact dose of urea solution required to meet a particular standard (i.e. Euro VI). Finally, this solution mixed with exhaust gases enter into the SCR (Selective Catalytic Reduction) unit. Inside this device a catalytic reaction is produced to convert NOx into diatomic nitrogen (N_2), and water (H_2O).

The parameters acquired from the ECU and the rolling bench are listed in Fig. 3. These data are crucial, as Full Throttle Pedal Position (FTPP), engine regime and the SCR inlet temperature are required to carry out the tests. The other data, such as EGH inlet and outlet temperatures (T_{B_EGH} and T_{A_EGH} respectively), the electrical power consumption of the heater ($P_{EGH} = \sqrt{3}\cdot V_{EGH}\cdot I_{EGH}\cdot cos\varphi$ being V_{EGH} the

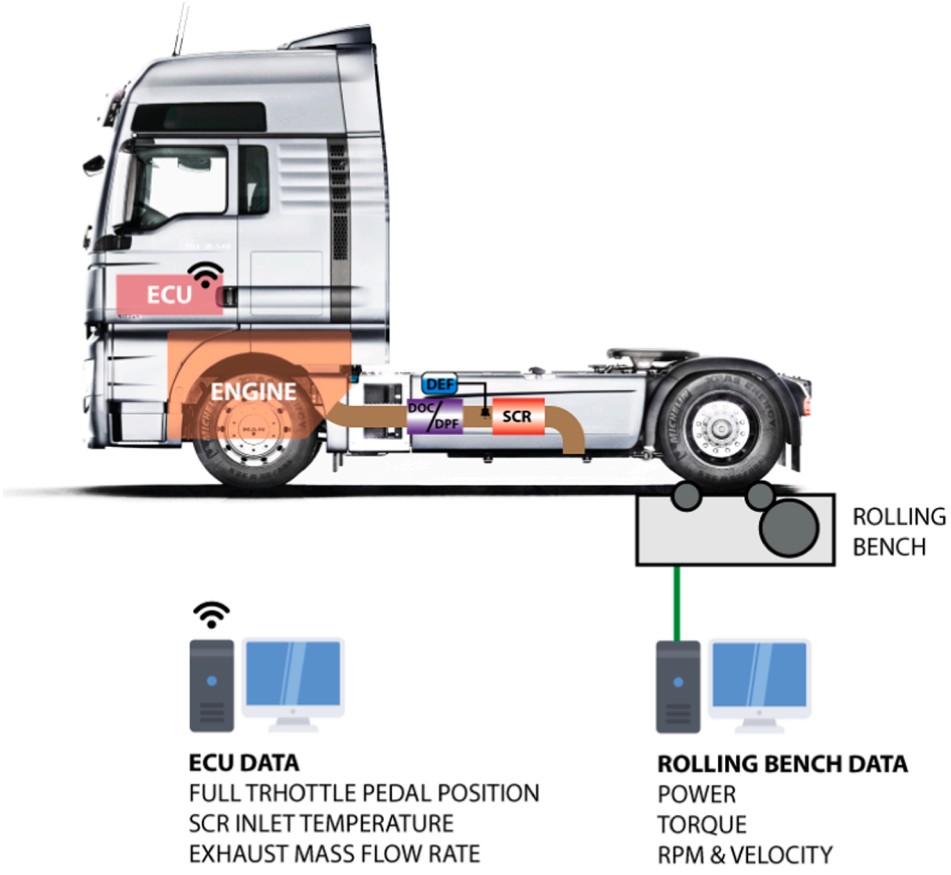

Fig. 3. Scheme of data acquisition obtained from ECU and rolling bench.

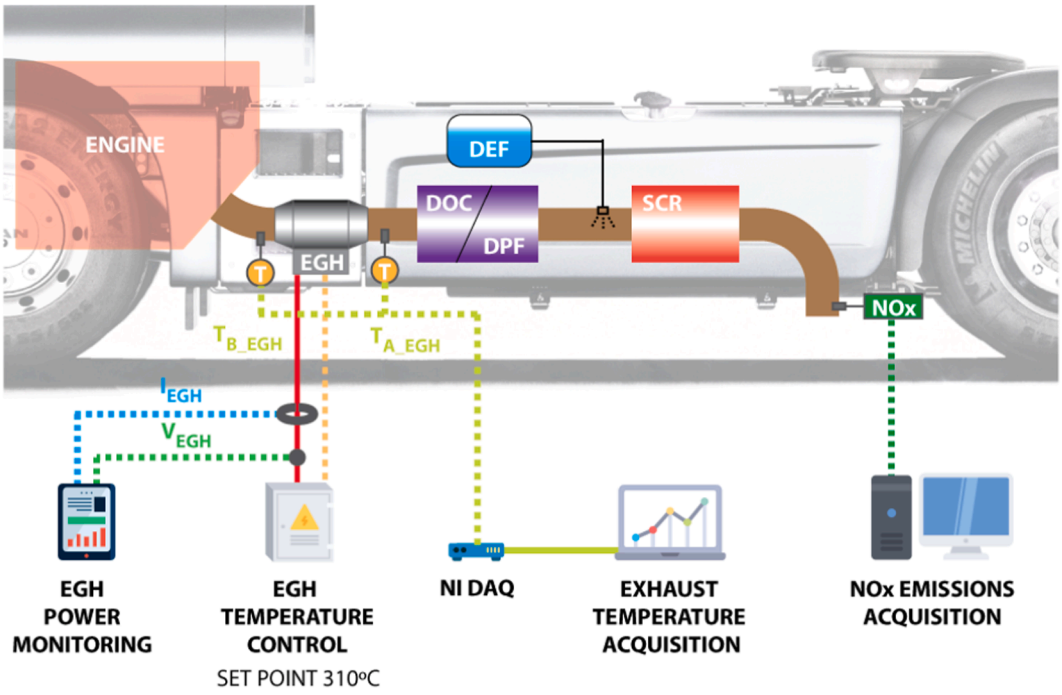

Fig. 5. Scheme of emissions reduction system in tested vehicle.

voltage and I_{EGH} the current) and NOx emissions (NOx_{EGH}) are obtained from external equipment. A scheme of these data acquisition can be seen in Fig. 5.

With this particular distribution of the components, it is presumable that a rise in exhaust gases temperature can increase the efficiency of the catalytic reaction into the SCR during cold start conditions and low demanding routes with frequent stops. Furthermore, this temperature rise represents a good effect for the DPF regeneration. This system could contribute to a more efficient fuel consumption, as extra doses of fuel may not be needed for burning particles inside the DPF. The most suitable place for the addition of an ATEG to harvest thermal energy is at the end of the standard SCR system, thus alterations of both flow and exhaust gas temperatures are minimized.

The location of the EGH during the test can be seen in Fig. 6, with minimal deviation of the original exhaust pipe in order to maintain the original vehicle design and to avoid gas flow alterations. Thermocouple sensors shown in Fig. 5 can be seen at inlet and outlet of the heating device. Temperatures before EGH (T_{B_EGH}) and after the EGH (T_{A_EGH}) are fundamental in order to analyse the performance of the proposed system.

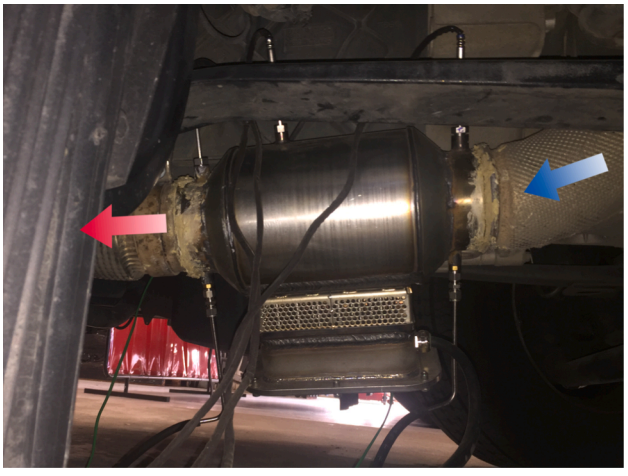

Fig. 6. EGH installation upstream of the aftertreatment system and gas flow direction.

A certified test bench for HDV (Maha Powerdyno R200/1) is used to simulate a real vehicle in specific use conditions. This equipment is also used to capture the FTPP from the ECU. Unfortunately, it was impossible to get the specifications of the on board acquisition system, so the accuracy of FTPP measure is not available. A MIAC G4.0 was used to measure NOx emissions at the end of the exhaust pipe. This device presents a measure range from 0 to +5000 ppm, an accuracy of ±5% of mv (+100 to +2000 ppm) and ± 5 ppm (0 to +99.9 ppm) with a resolution of 0.1 ppm (0 to +500 ppm). The equipment used to measure the EGH power consumption was a Dranetz Power Explorer PX5 power meter with the following specifications: voltage measuring range from 1 to 600Vrms with 0.1% rdg (reading) + 0.05% FS (full scale), 256 samples/cycle, 16 bit ADC; current measuring range from 1 to 6000Arms with 0.1% rdg + CTs (4), 256 samples/cycle, 16 bit ADC. Exhaust temperatures were recorded with a National Instruments DAQ with one NI 9211 acquisition module. This device presents a maximum measure error of 2.2 °C (0–400 °C) with a measurement sensivity < 0.07 °C. All temperature probes used were type K thermocouples.

The vehicle selected as an experimental unit was a MAN TGX 18.480. Its specifications are summarized in Table 1.

The rolling bench was configured with enough load to prevent rear tires from sliding while testing as seen in Fig. 7. All tests were made using the same load. This load can be considered irrelevant for the conclusions of the present work.

Three different stationary points were selected to conduct the study.

Table 1
Main specifications of tested vehicle.

Parameter	Value
Maker	MAN
Model	TGX 18.480 Efficient Line 2
Gearbox	Automatic (12 gears)
Max. rated power	353 kW (at 1800 rpm)
Max. rated torque	1500 Nm (at 930–1400 rpm)
Emission standard	Euro VI

Fig. 7. Vehicle position on the rolling bench during the experiment.

All of them presented low rpm values in order to analyse low demanding engine speed. The eleventh gear was selected to obtain all range of FTPP. Stationary regime was rapidly reached and stabilized in each particular test and only after this point data was registered. Engine temperature was always below 90 °C in order to keep the same engine conditions during the tests, simulating a cold start condition. A short period was held to reduce the engine temperature between tests. All regimes selected for this experiment, shown in Table 2, can be found in a typical daily drive. NOx emissions were analysed under the following engine regimes and FTPPs.

4. EGH experimental results

The first part of this section presents a comparative analysis of NOx emitted by a standard HDV, with and without the use of a 12 kW EGH. As explained in Table 2, this comparative analysis was divided into three different categories according to each engine regime: 1000 rpm (55 km/h), 1250 rpm (68 km/h) and 1500 rpm (82 km/h). In all regimes, the target temperature of the EGH was set to 300 °C.

Considering that a power consumption of 12 kW may be excessive for the electrical system of the vehicle, in the second part, a more realistic approach on EGH power consumption (P_{EGH}) is conducted. The objective is to determine the SCR efficiency improvement at different values of EGH power, from 0.5 to 5 kW [29]. These values will be useful to carry out the theoretical study of Chapter 5, where the viability of using a thermoelectric waste heat recovery system to supply the energy required by the EGH is studied.

4.1. Nox reduction analysis under different engine regimes

As it can be seen in Fig. 8, at 1000 rpm, the NOx ppm values are the highest of the three regimes (Figs. 8 to 10). NOx emissions, considering

Table 2
Stationary points selected for the tests.

Test	Engine regime (rpm)	FTPP (%)	Vehicle speed (km/h)
1	1000	30, 35, 40, 45, 50, 55, 60, 70, 80, 90	55
2	1250	30, 35, 40, 45, 50, 60, 70, 80, 90	68
3	1500	30, 35, 40, 45, 50, 60, 70, 80, 90	82

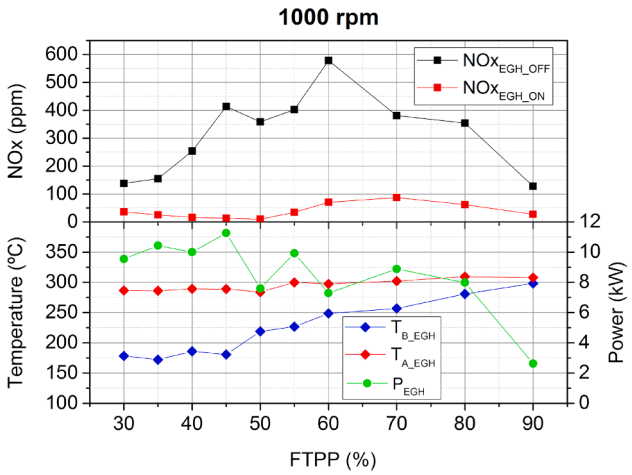

Fig. 8. NOx emissions with EGH on and off (upper graph) and exhaust gas temperatures before and after EGH with power consumed by EGH at 1000 rpm (lower graph) as a function of the FTPP. Note that error bars are smaller than the size of symbols.

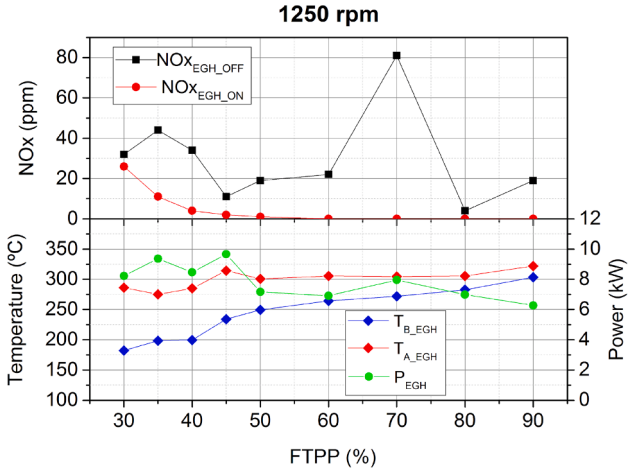

Fig. 9. NOx emissions with EGH on and off (upper graph) and exhaust gas temperatures before and after EGH with power consumed by EGH at 1250 rpm (lower graph) as a function of the FTPP. Note that error bars are smaller than the size of symbols.

that EGH was disabled NOx_{EGH_OFF}, achieved 578 ppm when the FTPP was at 60%. At the same conditions, NOx measured with the EGH enabled NOx_{EGH_ON} was about 87 ppm. This was the maximum reduction achieved in all tests. In absolute numbers, it represented a NOx reduction of 508 ppm. In relative terms, however, the greatest reduction was achieved at 50% FTPP with 97.2% of ppm reduction.

Detail analysis of Fig. 8 reveals that inlet and outlet EGH temperatures, T_{B_EGH} and T_{A_EGH}, converged at high FTPP values. This can be explained by the higher exhaust gas temperatures generated by the combustion engine that made the EGH to turn off for temperatures higher than 300 °C (note that the setpoint temperature of the EGH was set to 300 °C). A dramatic decrease in NOx emissions was obtained at 60% FTPP when the EGH was disabled. As mentioned before, urea solution is dosed over 180 °C. This means that a NOx reduction should have been registered at 50% FTPP and above. However, NOx emissions start to fall at 60% FTPP. This short delay (15 s in the experiment) can be related to ECU parameters that control the exact moment of dosing. Note that EGH was not needed at maximum FTPP where the power demand by the EGH was effectively reduced below 3 kW. Contrarily, at low engine loads (i.e. FTPP < 80%), EGH consumed much more power to

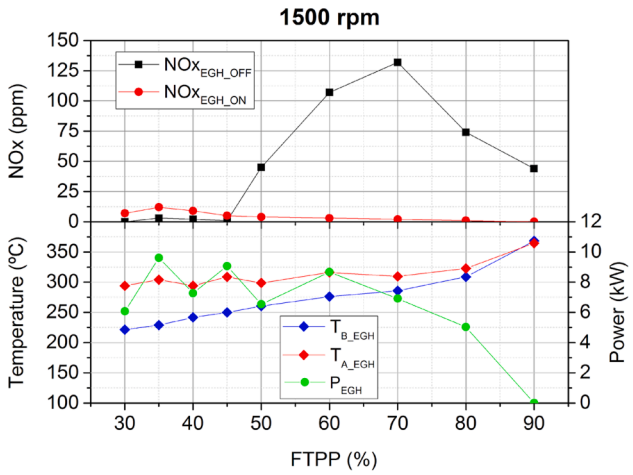

Fig. 10. NOx emissions with EGH on and off (upper graph) and exhaust gas temperatures before and after EGH with power consumed by EGH at 1500 rpm (lower graph) as a function of the FTPP. Note that error bars are smaller than the size of symbols.

increase the exhaust gas temperature to the desired set point. Consider that the exhaust mass flow rate tends to increase with FTPP. That is the reason why the power consumed by the EGH at 80% FTPP is the similar to 60% FTPP, despite having different inlet temperatures. Peak power consumption P_{EGH} of 11.26 kW is reached at 45% FTPP obtaining a NOx reduction of 400 ppm. For medium range FTPP values, P_{EGH} is being slowly reduced as exhaust gas temperatures tend to stabilize around 300 °C.

In Fig. 9, at 1250 rpm, it can be observed that EGH also permitted a reduction of NOx emissions. However, in this case the NOx values with the EGH turned off (NOx_{EGH_OFF}) substantially decreased in comparison with the previous regime at 1000 rpm (Fig. 8). This tendency is also observed at 1500 rpm although in a less pronounced way (see Fig. 10). At 1250 rpm the NOx_{EGH_OFF} peak was reached at 70% FTPP with a value of 81 ppm. This stationary point presented a NOx reduction of almost 100% after enabling the EGH. It represents the most relevant NOx reduction at 1250 rpm in absolute numbers. At this regime, an almost completely reduction of NOx started at 60% FTPP and it was maintained for higher FTPP values. On the other hand, the same behaviour as in 1000 rpm, regarding the temperature convergence at high FTPP values, was observed. Both EGH inlet and outlet gas temperature curves took the same tendency at the end of the test with a difference of just 18.5 °C at 90% FTPP. It also can be appreciated a coincidence between the peak demand (9.66 kW) at 45% FTPP and the peak of T_{A_EGH} (314.33 °C). After this value, power decreased and T_{A_EGH} was stabilized until 80% FTPP. The EGH power consumption was 7.95 kW at the major NOx reduction point found at 70% FTPP (81 ppm).

Fig. 10 shows the stationary points at 1500 rpm. It can be observed that the contribution of the EGH was non-existent along the first FTPP points. Note that NOx emissions are higher when EGH is turned on than off. This can be explained by the EGR valve aperture at the 30%-45% FTPP that cut NOx emissions through the reinjection of the exhaust gases into the admission port. ECU controls the valve opening angle and may be slightly different in the two tests. On the other hand, it was at FTPP values higher than 45% when the EGH contribution was relevant. A NOx_{EGH_OFF} peak point of 132 ppm at 70% FTPP was observed. These NOx emissions NOx_{EGH_ON} were reduced up to 98.48% through the use of the EGH.

The major difference between T_{B_EGH} and T_{A_EGH} was achieved at the beginning of this test (30% FTPP). This initial heating led to very low NOx_{EGH_ON} values during the entire test, despite not being as low as NOx_{EGH_OFF} values until 45% FTPP. Overall, this test registered a total NOx reduction of 89.46% and this was achieved specially at middle FTPP range with a significant power consumption (6.5 kW – 8.5 kW). Regarding both EGH inlet and outlet temperature curves we can see a steady increase after 50% FTPP. This is because in mid-high demanding regimes, such as 1500 rpm, the engine produces great amounts of thermal energy that produces high exhaust gas temperatures. This particular regime is an example where EGH is less required because combustion engines produce enough heat to make the catalytic conversion highly efficient, see Fig. 1. Notice the dramatic decrease of P_{EGH} at the last third of the test.

Regarding the power consumption of EGH, there was a tendency repeated in all three tests. There was a huge amount of energy required to rise temperatures in a short period, for the first half of stationary points studied. As FTPP increased for the same regime, temperatures of the exhaust gas also increased and EGH power demand decreased drastically at the end of each test. The lowest point of instant power demand was always at 90% FTPP.

A common pattern was detected through the three studied regimes. Without EGH, the NOx_{EGH_OFF} peak was reached between 60 and 70% FTPP. However, thanks to the inclusion of the EGH, the urea solution injection threshold was reached earlier. Consequently, the earlier catalytic conversion provided a dramatic descend of NOx_{EGH_ON}.

Results in Figs. 8 to 10 include the absolute uncertainty values of measured data. NOx and temperature standard uncertainties have been calculated using the measurement accuracy obtained from the manufacturer's datasheet (see Chapter 3). Note that EGH power was indirectly obtained by the product of voltage and current, separately read with the power meter. Then, the measurement uncertainty of EGH power was calculated combining the uncertainties in measured parameters to arrive at an uncertainty value for an experimental result that depends on these parameters [30,31]. However, the error bars of data are <5% for all cases and may be even lower than the size of the symbol used in the graphs.

In Table 3, the overall results of NOx reduction are summarized. Achievements are remarkable in all cases being the less average reduction obtained in Test 3 (53.94%). This result is mainly due to the high exhaust gas temperatures produced by the engine at 1500 rpm. These high temperatures make the SCR conversion more efficient without the need of an EGH. We must take into account there was higher NOx emissions NOx_{EGH_OFF} at 1500 rpm compared with the 1250 rpm regime. On the other hand, if we sum comparative ppm values of all FTTP cases in each regime, we can observe that Test 1 gave the best result of total NOx reduction (2780 ppm). Furthermore, all tests presented results over 80% in total NOx reduction. This indicates the important role of the EGH to eliminate a significant quantity of NOx at low engine regimes.

However, there is an issue that needs to be analysed in more detail. As seen in Table 3, power consumption is far beyond maximum capabilities of an EGH connected to an ATEG. The main goal of the following subsection is to establish a compromise between SCR efficiency at low temperatures and the power consumed by the EGH providing the energy demand requirements in order to design a suitable ATEG.

4.2. EGH power consumption vs SCR efficiency

Thermoelectric generators can reach efficiencies of 5%. These efficiencies can only be achieved when TEGs are subjected to its maximum temperature difference [32–35]. However, when TEGs are

Table 3
Comparative NOx reduction results in different tests.

TEST	Average NOx reduction (%)	Total NOx reduction (%)	Total NOx reduction (ppm)	Average EGH power consumption (kW)
1	86.35	87.97	2780	8.55
2	84.28	83.45	222	7.89
3	53.94	89.46	365	6.58

interconnected between them and located along the exhaust pipe, last modules are subjected to lower temperature differences than first modules, producing a decrease on the overall efficiency of the ATEG [36,37]. As seen in current research, ATEG systems can achieve effective efficiencies around 2,5% [28]. Thus, it is necessary to determine if an ATEG can supply the energy demanded by the EGH. In this section, a feasibility study on EGH power as well as energy consumption is conducted. It is possible to determine the SCR efficiency improvement for different P_{EGH} using the SCR conversion efficiency data from Fig. 1, the experimental SCR inlet gas temperatures (T_{IN_SCR}) and exhaust mass flow rate ($\dot{m}$) obtained from the ECU.

Test 1 scenario will be used for this theoretical approach due to its low engine regime (1000 rpm) and its low gas temperatures that reflect a typical low speed route done by a HDV. Selected FTPP values are in the low range (30%-45%) because it is where the T_{B_SCR} are lower than the urea solution threshold (T < 180 °C). Data in Table 4 contains a SCR inlet gas temperature comparison between the standard system (EGH disabled), the same system with the EGH enabled, and a proposed EGH. This last group of gas temperatures is calculated using the heat transfer equation $P_{EGH} = \dot{m}c_p(T_{A\_EGH} - T_{B\_EGH})$ by assuming that all electrical power supplied to the EGH is effectively transferred to the exhaust gases in terms of heat. In the previous equation,P_{EGH} is the proposed power of the EGH, $\dot{m}$ is the measured exhaust gas mass flow rate at a constant FTPP, c_p is the specific heat at constant pressure of the exhaust gases calculated using the temperature value registered for each FTPP, and T_{B_EGH} is the measured exhaust gas temperature before the EGH at a constant FTPP. As seen in Chapter 3, the SCR is installed downstream the EGH. For this reason, we consider $T_{A\_EGH} = T_{B\_SCR}$. Table 4 shows the SCR efficiency improvements under different values of P_{EGH}, ranging between 0.5 and 5 kW.

As seen in Table 4, low P_{EGH} provides a slightly increase in exhaust gas temperatures that leads to a moderate benefit in SCR conversion efficiency. P_{EGH} values below 2 kW only contribute to increase the SCR efficiency about 3% to 7%. SCR efficiencies up to 80% can be found at 40 FTPP with a P_{EGH} of 2 kW. To conclude these comparative results, it is clear that 95% of SCR efficiency needs EGH consumption values between 4 kW and 5 kW.

These results demonstrate that the standard SCR performed at 60–68% of its efficiency. It is interesting to note that the lowest FTPP (30%) value is not the poorest in efficiency terms. In the same way, the highest FTPP (45%) is not the best performing regarding power consumption values. Maximum efficiency (95%) is reached firstly at 40% FTPP with 4 kW consumed.

At this point it is important to remark that it is unnecessary to consume 12 kW in an EGH to substantially reduce NOx emissions. Considering temperature of urea solution injection around 180 °C, it is clear that the EGH device should only heat the exhaust gases up to reach this target value. To provide an extra thermal power to the exhaust gases is useless and counter-productive. The SCR efficiency reaches its maximum in the worst FTPP scenario of low exhaust gas temperatures with a 5 kW EGH.

In a conventional system, the power supplied as well as the energy consumed by the EGH must be extracted from the electrical system of the vehicle. The electrical power generated by the vehicle comes from the alternator, which converts part of the mechanical energy produced by the combustion engine into electricity. This means that a system with EGH to achieve an extra NOx reduction would demand more electrical energy. Hence, more time using the alternator would imply an increase on the vehicle's fuel consumption.

To avoid this emission increment, our research focuses on the viability of using the exhaust waste heat to produce the electricity needed for the EGH. The goal is to simulate and quantify an ATEG model to convert waste heat, downstream of the aftertreatment system, into electricity. This will avoid the need for the electric system to consume more fuel to produce the extra electrical energy. Many theoretical models [27,28,37–39] and experimental prototypes [40–44] have been developed which demonstrate the feasibility of automotive ATEGs. Other ways to produce this additional energy from exhaust gases may be

Table 4
SCR efficiency for different EGH powers at 1000 rpm.

	SCR inlet temperature (T_{B_SCR})			SCR conversion efficiency		
FTPP (%)	EGH disabled (°C)	Tested EGH enabled (°C)	Proposed EGH enabled (°C)	EGH disabled (%)	Tested EGH enabled (%)	Proposed EGH enabled (%)
EGH proposed of 0.5 kW						
30	178.27	286.41	183.94	64%	95%	67%
35	172.15	286.1	177.63	60%	95%	63%
40	185.9	289.13	191.09	68%	95%	72%
45	180.7	288.82	185.58	65%	95%	68%
EGH proposed of 1 kW						
30	178.27	286.41	189.61	64%	95%	71%
35	172.15	286.1	183.11	60%	95%	67%
40	185.9	289.13	196.28	68%	95%	75%
45	180.7	288.82	190.46	65%	95%	71%
EGH proposed of 2 kW						
30	178.27	286.41	200.96	64%	95%	78%
35	172.15	286.1	194.07	60%	95%	74%
40	185.9	289.13	206.66	68%	95%	82%
45	180.7	288.82	200.21	65%	95%	78%
EGH proposed of 3 kW						
30	178.27	286.41	212.30	64%	95%	85%
35	172.15	286.1	205.04	60%	95%	81%
40	185.9	289.13	217.04	68%	95%	88%
45	180.7	288.82	209.97	65%	95%	84%
EGH proposed of 4 kW						
30	178.27	286.41	223.65	64%	95%	93%
35	172.15	286.1	216.00	60%	95%	88%
40	185.9	289.13	227.42	68%	95%	95%
45	180.7	288.82	219.72	65%	95%	90%
EGH proposed of 5 kW						
30	178.27	286.41	234.99	64%	95%	95%
35	172.15	286.1	226.96	60%	95%	95%
40	185.9	289.13	237.79	68%	95%	95%
45	180.7	288.82	229.48	65%	95%	95%

the use of Organic Rankine Cycle (ORC) [45–47].

5. ATEG simulation model

In order to validate the previous exposed idea, a simulation model of an ATEG is launched with relevant data gathered during the experimental test described in Section 3. The idea is to explore the theoretical capabilities of commercial Thermoelectric Modules (TEM) disposed in a particular array that guarantees enough power to supply electrical energy to the EGH. Focusing on this goal, a 1500 rpm regime is chosen as it contains the highest tested exhaust gas temperatures without surpassing the TEM maximum working temperature (230 °C). As explained in Section 4.2, EGH may not be needed with high exhaust gas temperatures at this regime. On the other hand, ATEG benefits from these conditions to convert thermal energy into electricity for a future use in a low regime (for example 1000 rpm).

GT-SUITE [48] is chosen as the simulation software due to its proven research in the automotive sector [36,42,49–52]. This multiphysics CAE simulation tool is a commonly used software for engine modelling, which also incorporates a TEG block in its library to model and size automotive thermoelectric generators for exhaust waste heat recovery. This software has been validated with experimental data in multiple references [42,49,50]. Despite our specific configuration proposed, exhaust systems of internal combustion engines have been successfully simulated and validated with this tool. For example, Massaguer et al. [36] compared and validated a longitudinal thermoelectric energy harvester (LTEH) by using a mathematical model and experimental data. Furthermore, Cózar et al. [50] successfully reproduced the performance curve of the same commercial TEM (Marlow TG12-8-01LS) used in our simulation model.

Exhaust gas temperature and its mass flow rate are both variables depending on a particular FTPP value. It is important to keep in mind the most suitable location for an ATEG into the exhaust system of this particular vehicle. During the thermoelectric energy conversion, the ATEG reduces the temperature of the exhaust gases, the opposite effect to what is sought inside the ATS. Having this in mind, the best location of the ATEG is downstream of the ATS. This location allows us to conclude that the exhaust inlet temperature parameter introduced into the simulation is going to be the SCR outlet temperature obtained from the ECU during the experimentation. On the other hand, there are constant parameters introduced such as coolant mass flow rate (0.12 kg/s) and coolant inlet temperature (25 °C). This cooling circuit relies on a water pump and a heat exchanger that provides a constant flow along the cold face of every TEM. Ambient temperature registered from the day of the experiment (30 °C) is introduced for the TEM initial temperature parameter. Table 5 provides a general overview of the different case studies of this ATEG simulation. Each case study represents a particular FTPP analysed with the HDV on real conditions. Notice that ATEG inlet temperatures correspond to data registered at the end of the standard exhaust system tested, as is the optimal position for coupling this ATEG component.

The thermoelectric module used in the simulation was the TG-12–08 from Marlow Industries. This module uses bismuth telluride as a thermoelectric material. It was chosen because it has shown a high correlation between manufacturer's data and experimental data [36]. Apart from that, its maximum working temperature is 230 °C, which is very similar to the average engine exhaust temperatures. The TG-12–08 has the following dimensions 44.7 × 40.3 × 3.53 mm (LxWxH). The external contact plates are made of aluminum oxide to electrically insulate the inner circuit.

To carry out the simulation, it is necessary to obtain the characteristic parameters of the thermoelectric module and enter them into the software. These are: the seebeck coefficient, the thermal resistance and the electrical resistance of the TG-12-08 at different average temperatures T_{avg}. Thermoelectric average temperature T_{avg} is calculated in °C as follows: $T_{avg} = (T_H + T_C)/2$ where T_H is the hot side temperature and T_C is the cold side temperature of the module.

Using the manufacturer data, a regression line is obtained for each parameter, Eq. (1) to (3), which give a high coefficient of determination R^2 greater than 0.95. These linear equations are then used by the software to find new values.

Seebeck coefficient [mV/K]

$$\alpha = (-4.142\hat{A}\cdot 10^{-2})\hat{A}\cdot T_{avg} + 58.26 (R^2 = 0.95) \quad (1)$$

Thermal resistance [K/W]

$$R_t = (-1.3293\hat{A}\cdot 10^{-3})\hat{A}\cdot T_{avg} + 1.314 (R^2 = 0.98) \quad (2)$$

Electrical resistance [Ω]

$$R_i = (9.2738\hat{A}\cdot 10^{-3})\hat{A}\cdot T_{avg} + 1.4579 (R^2 = 0.99) \quad (3)$$

The above exposed calculations are considered close enough to experimental data regarding R^2 values (0.95–0.99). Thus, it is considered that TEM parameters are reliable and ATEG simulation can provide a theoretical model close to reality.

Finally, to simplify the model, the following parameters have been neglected:

- Contact resistance between elements.
- Convective and radiative heat losses in the TEG.
- Thomson effect. This effect has a very low impact in TEG performance, typically two times less than the Joule effect [53]. This work [54] rigorously demonstrates that the standard thermoelectric model, neglecting Thomson effect, produces the exact module output power and efficiency if an integral-averaged Seebeck coefficient is used.

TEMs form an electrical array as shown in Fig. 11. Each cell is represented by a voltage source $V_{1,\ldots,180}$ and an internal resistance $R_{1,\ldots,180}$. To begin with, 15 TEMs are connected in series. Afterwards, this pattern is repeated in 12 parallel rows up to a total number of 180 thermoelectric units. The ATEG can operate under two system stages as exposed in Chapter 2. Heating stage (1) is activated when the system increases the exhaust gas temperatures by means of the EGH to improve the SCR efficiency. As represented, PCU controls the electrical energy delivery from the battery. Recovery stage (2) transforms waste heat into electrical energyand the PCU stores it into the battery for future uses. This ATEG electrical configuration is designed to obtain a proper relationship between current and voltage to feed the PCU converter. In order to charge correctly the battery, voltage is stabilized at 12.8 V.

The distribution and assembly of the different TEMs is taken from a trusted model already tested in a car [25]. The full TEM assembly contained in the simulated ATEG appears in Fig. 12. Its square shape is used to pack them in four rows of 15 TEM each. This composition is repeated in three subassemblies. Hot sides of TEMs are the interior ones where exhaust gas is canalized. Cold sides of TEMs are the exterior ones for its refrigeration using cold plates. Notice the counter-flow disposition between exhaust gas and coolant.

Table 5
Exhaust gas parameters in different FTPP values.

CASE STUDY	FTPP (%)	Exhaust mass flow rate (kg/h)	ATEG inlet temperature (°C)
1	30	313.2	242
2	35	474.7	223
3	40	513	201
4	45	541.7	186
5	50	636.5	186
6	60	789.2	196
7	70	1013.2	214
8	80	1315.7	249
9	90	1315.7	295

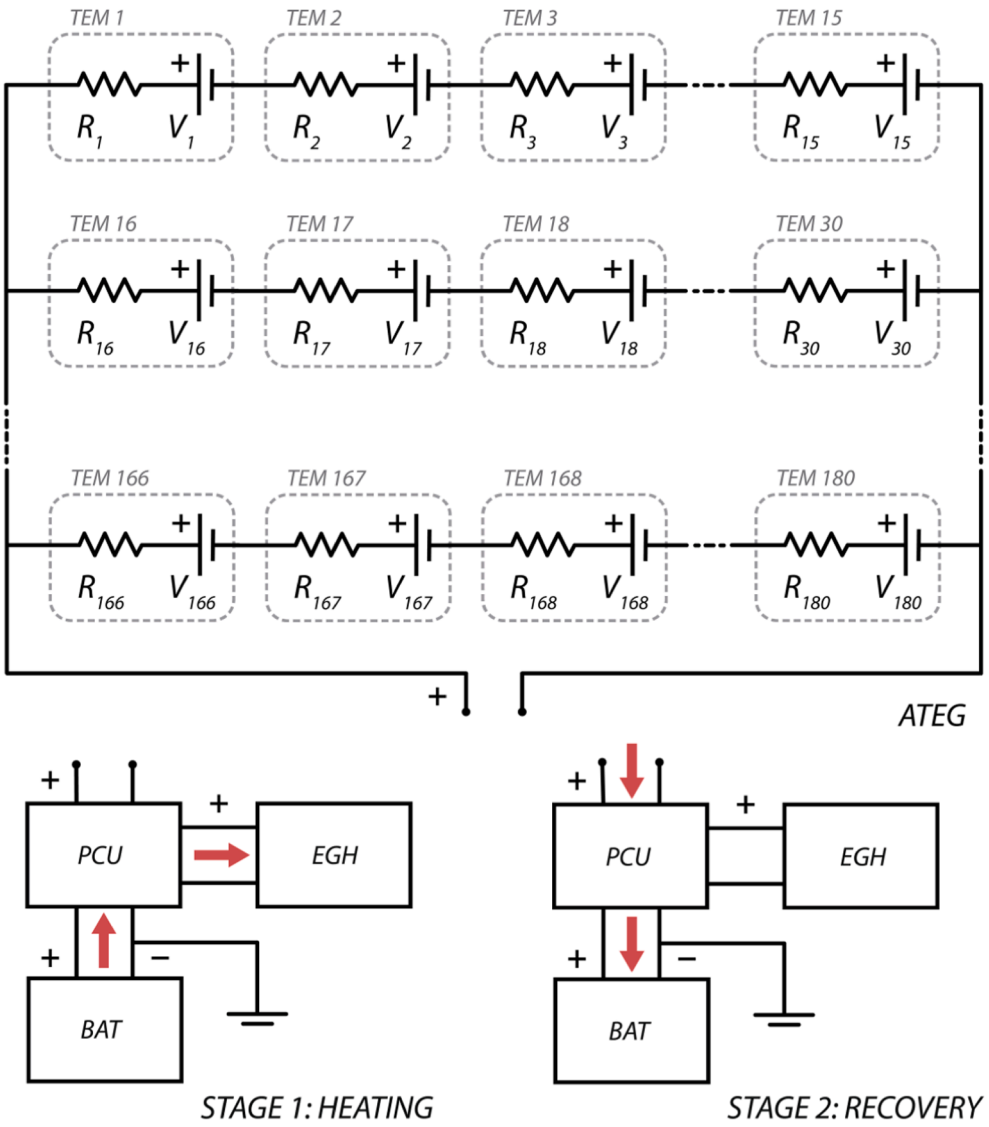

Fig. 11. Simulated electrical scheme of system proposed. Includes ATEG with its TEM array, Heating stage (1) and Recovery stage (2) with its particular energy flow between battery, PCU, EGH and ATEG.

Heat exchange geometry applied to the model, is also taken from the same trusted model mentioned before. The hot side heat exchanger is composed of a holed aluminium block. This block has 5 identical holes through which exhaust gases flow. The interior cross-sectional area of each hole is 25 mm^2 and the wetted perimeter of the pipe, used in the calculation of the hydraulic diameter, is 58 mm. The surface roughness of the pipe is 0.002 mm, corresponding to drawn metal. The same geometry is used for the cold side heat exchanger.

The simulation uses Chilton Colburn analogy to calculate the heat transfer coefficient of each case study, as it is the recommended option for laminar and liquid–gas flow simulation [55].

Heat transfer coefficients obtained are within standard values (400–1500 W/m^2K) and demonstrate that the simulation is reliable. Finally, we can have a precise lecture of the amount of energy recovered from the waste heat of this exhaust system. It covers a wide range of values (0.4–1.4 kW) depending on the FTPP analysed.

It is important to note that the energy loss due to backpressure on the exhaust pipe and pressure loss in the cold side heat exchanger have not been considered. Following the considerations exposed in [27,41,42], the energy loss due to this two phenomenon should be subtracted from the power generated by ATEG to obtain the net power generated.

A correlation of time can be established to supply the demanded power P_{EGH} , shown on Table 4, with the simulation results seen in Table 6. Here, test route conditions of a HDV are considered combining both stages of the system proposed using regime and speed data gathered from the previous tests. For the heating stage, we have selected the worst regime for SCR efficiency values (1000 rpm, 50 km/h). Indeed, it is during this cold start conditions when all the electric energy stored in the system must be transformed into heat using the EGH. For the recovery stage, the engine regime is set to 1500 rpm (80 km/h). With this route parameters, exhaust wasted energy is recovered by the ATEG and stored for being used in future EGH demands.

It is assumed that EGH is used the first 12 min after the engine start up. This time conicides with the cold start period for this particular vehicle. After this is time, the standard aftertreatment system of the vehicle starts cutting NOx emissions efficiently. Fig. 13 shows the working period required by the ATEG at 1500 rpm (recovery stage) to supply enough energy to the EGH (heating stage) during cold start. In addition, the recovery stage time depends on FTPP (%) and target power of the EGH (kW).

Regarding these results, it is observed a common pattern with two different zones. If we are moving into the lower range of FTPP (30%-45%), the recovery time needed for an ATEG is considerably long, as exhaust gas temperatures are too low to generate a great amount of

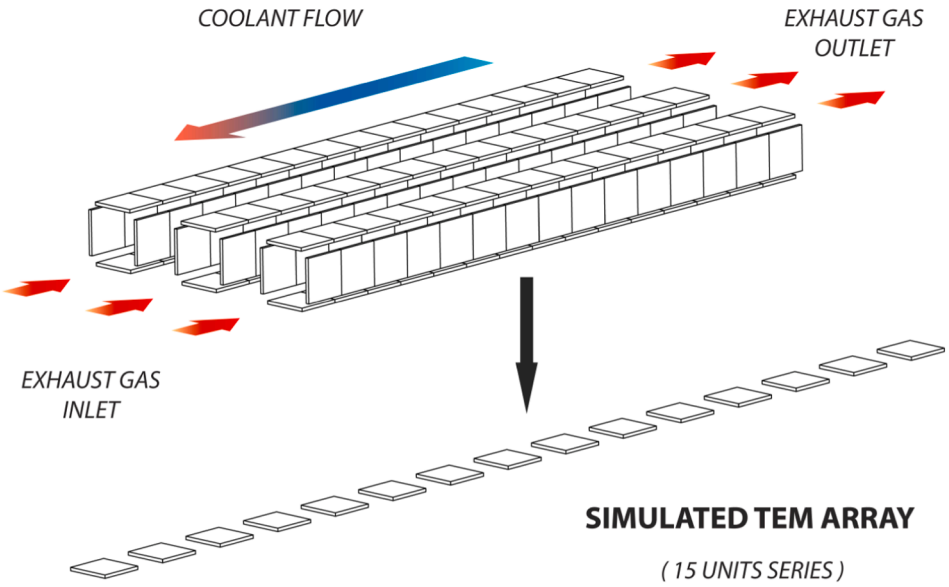

Fig. 12. TEM distribution and total composition of theoretical ATEG simulated.

Table 6
Relevant data from ATEG simulation results.

CASE STUDY	Power (W)	Voltage (V)	Exhaust Outlet Temperature (°C)	Coolant Outlet Temperature (°C)	Heat Transfer Coefficient (W/m^2K)
1	425.22	36.22	64.72	28.42	409.41
2	514.21	41.85	87.58	28.95	549.85
3	442.68	38.67	85.55	28.64	574.78
4	392.40	36.28	83.59	28.41	592.88
5	435.70	38.73	92.78	28.64	667.42
6	546.68	44.25	109.67	29.17	786.05
7	729.58	52.32	133.90	29.96	955.78
8	1063.12	65.11	170.64	31.27	1183.07
9	1428.72	77.43	199.94	32.64	1213.10

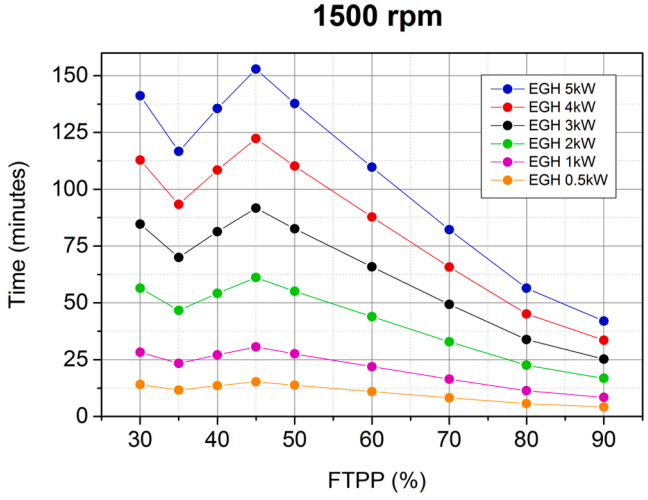

Fig. 13. Time using ATEG to supply EGH power demand during cold start period at 1500 rpm.

power in a short period of time. Obviously the 5 kW EGH is the longest to get fully supplied with 152 min if we consider that the ATEG is working continuously at 45% of FTPP. On the contrary, remaining with the same FTPP, it takes only 15 min to achieve its aim if the EGH supplies 0.5 kW.

The second zone of the graphic shows a progressive descend in the time needed to power the EGH. With higher FTPP values, the exhaust gas temperatures are higher. Consequently, the ATEG energy recovered is also higher. This explains why less time of ATEG operation is needed with higher FTPP values. For a 0.5 kW demand, it needs<5 min of the vehicle at 1500 rpm and 90% FTPP. Moving to the higher FTPP band, only 41 min is needed to fully supply an EGH of 5 kW.

As seen before, the majority of time figures are possible to achieve during a normal long-haul working journey of a HDV. However, it is important to add some light to the emission reductions obtained with this ATEG coupled to different EGH power configurations. Fig. 14 quantifies the SCR efficiency improvement of the proposed EGH + ATEG system respect to the standard aftertreatment system of the HDV tested, both cases compared at 1000 rpm regime. Y-axis (time values in minutes) represents the duration of the recovery stage performed by the ATEG at 1500 rpm regime. These results confirm that EGH is required in lower or medium FTPP values, where major improvements are achieved, especially at high power demand of EGH (4 kW – 5 kW). Analysing results from high FTTP values to lower, we can see a progressive increase in SCR improvement, related with EGH power demand. From 65% FTPP

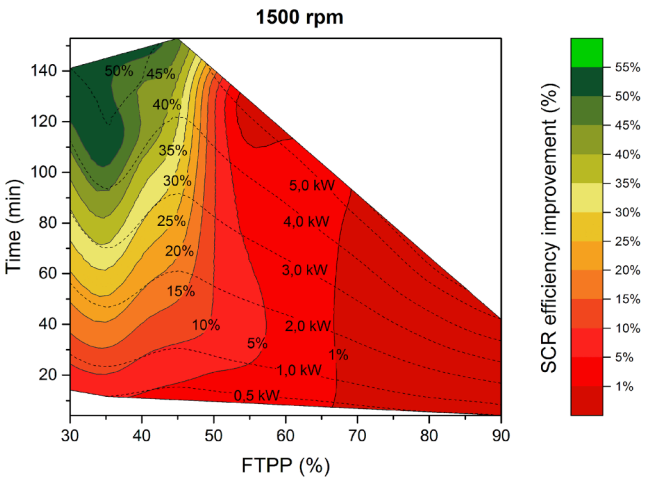

Fig. 14. SCR efficiency improvement at 1000 rpm using different EGH power. Time using ATEG at 1500 rpm to supply respective EGH power demands at 1000 rpm.

onwards there is no remarkable efficiency improvement (<1%) of the catalytic system. Even for an EGH proposed of 0.5 kW, we can see that improvements in almost every FTTP can be dismissed. A poor efficiency improvement (5%-15%) is obtained for FTPP downwards until 50% for most EGH power values. However, EGHs of 0.5 kW and 1 kW are included totally in this improvement zone or even lower. The next efficiency improvement zone is more dynamic, which represents major values obtained adding few extra minutes of the ATEG recovery stage. Observing this medium improvement zone (15%-40%), we can conclude that includes low FTPP values (30%-45%). EGH power demand required for these improvements is in the range of 2 kW to 3 kW. The time needed to recover this energy through the ATEG is moderate (approximately 50–90 min). Moving on, we arrive to major recovery improvements (40%-55%). These figures can be obtained by EGH power values of 4 kW to 5 kW and can be applied for low FTTP values (30%-45%). Time figures for recovery stage of this power range are longer (95–155 min) but completely within HDV daily transportation routines.

6. Conclusions

This study experimentally demonstrates that the use of an EGH can reduce the NOx emissions more than 80% in a Diesel-powered Euro VI Heavy Duty truck working at low engine regimes. The highest reductions were achieved at 1000 rpm and medium FTPP values. It also has been demonstrated that, at low engine regimes, EGH power higher than 5 kW does not produce a significant impact on NOx reduction. A conventional catalytic device heated using an EGH of 5 kW could improve the SCR efficiency from 65% to 95%. Consequently, exhaust gas heaters are a potential solution to the high emitting low engine regimes issue.

Numerical simulation of an ATEG demonstrate the viability of using the exhaust waste heat to produce electricity needed by the EGH. The designed ATEG layout consists of 180 commercial TEM units, distributed in 12 parallel groups of 15 consecutive cells. This ATEG generates a power range between 0.4 kW (at 30% FTPP) and above 1.4 kW (at maximum FTPP of 90%). These values are obtained using an average engine regime (1500 rpm) scenario. Thinking about greater values of power generated by the same supposed ATEG is not reckless as HDV engine maximum power of this particular unit is reached between 1600 rpm and 1800 rpm.

The viability of energy supply during a cold start scenario (1000 rpm during 12 min) is positively demonstrated by time figures not exceeding of 155 min in the worst conditions possible (5 kW of EGH demand and generation at 45% FTPP). This viability guarantees the needed increment for exhaust gas temperature (T_{B_SCR}) in order to warm up SCR and start dosing urea solution in a shorter period of time. In consequence, the SCR efficiency is improved up to 55% using a proposed EGH of 5 kW and powered exclusively by an ATEG.

Deeper research concerning ATEG optimization for HDV specific characteristics is needed. Future work must focus on the system design, providing an accurate net energy balance after considering exhaust backpressure and pressure loss. Design geometry is fundamental to minimize backpressure as internal sharp edges tend to influence into mass flow rate behavior.

It is also important to quantify cost and efficiency ratios in long haul case studies as they are the most common routes for these vehicles. At the same time, it is fundamental to make a calculation of the amount of energy generated with these optimized ATEG during a usual working period of time. Cold start scenarios could benefit for this electricity stored and generated when exhaust gas temperatures are optimal.

CRediT authorship contribution statement

J. Ximinis: Conceptualization, Methodology, Investigation, Writing - original draft. **A. Massaguer:** Conceptualization, Investigation, Supervision, Writing - review & editing. **T. Pujol:** Supervision, Writing - review & editing. **E. Massaguer:** Software, Supervision, Writing - review & editing.

Declaration of Competing Interest

The authors declare that they have no known competing financial interests or personal relationships that could have appeared to influence the work reported in this paper.

Acknowledgment

We would like to thank Fundación Repsol and EVARM INNOVACION SL for their support.

References

[1] Kalghatgi G. Is it really the end of internal combustion engines and petroleum in transport? Appl Energy 2018;225:965–74. https://doi.org/10.1016/j.apenergy.2018.05.076.
[2] Mera Z, Fonseca N, López JM, Casanova J. Analysis of the high instantaneous NOx emissions from Euro 6 diesel passenger cars under real driving conditions. Appl Energy 2019;242:1074–89. https://doi.org/10.1016/j.apenergy.2019.03.120.
[3] K. Ghasemzadeh, S.M.S. Tilebon, A. Basile, Conventional systems for exhaust gas cleaning and carbon capture and sequestration, in: Curr. Trends Futur. Dev. Membr., Elsevier, 2020: pp. 65–96. https://doi.org/10.1016/b978-0-12-817807-2.00004-6.
[4] Kim JY, Ryu SH, Ha JS. Numerical prediction on the characteristics of spray-induced mixing and thermal decomposition of urea solution in SCR system. In: Proc. 2004 Fall Tech. Conf. ASME Intern. Combust. Engine Div.; 2004. p. 165–70. https://doi.org/10.1115/icef2004-0889.
[5] Grigoratos T, Fontaras G, Giechaskiel B, Zacharof N. Real world emissions performance of heavy-duty Euro VI diesel vehicles. Atmos Environ 2019;201:348–59. https://doi.org/10.1016/j.atmosenv.2018.12.042.
[6] He L, Hu J, Zhang S, Wu Y, Guo X, Guo X, et al. Investigating real-world emissions of China's heavy-duty diesel trucks: Can SCR effectively mitigate NOx emissions for highway trucks? Aerosol Air Qual Res 2017;17(10):2585–94. https://doi.org/10.4209/aaqr.2016.12.0531.
[7] Kröcher O. Selective catalytic reduction of NOx. Catalysts 2018;8:459. https://doi.org/10.3390/catal8100459.
[8] Brack W, Heine B, Birkhold F, Kruse M, Deutschmann O. Formation of Urea-Based Deposits in an Exhaust System: Numerical Predictions and Experimental Observations on a Hot Gas Test Bench. Emiss Control Sci Technol 2016;2(3):115–23. https://doi.org/10.1007/s40825-016-0042-2.
[9] Zhao J, Wang J. Integrated Model Predictive Control of Hybrid Electric Vehicles Coupled with Aftertreatment Systems. IEEE Trans Veh Technol 2016;65(3):1199–211. https://doi.org/10.1109/TVT.2015.2405918.
[10] Gao J, Chen H, Li Y, Chen J, Zhang Y, Dave K, et al. Fuel consumption and exhaust emissions of diesel vehicles in worldwide harmonized light vehicles test cycles and their sensitivities to eco-driving factors. Energy Convers Manag 2019;196:605–13. https://doi.org/10.1016/j.enconman.2019.06.038.
[11] Guo J, Ge Y, Hao L, Tan J, Peng Z, Zhang C. Comparison of real-world fuel economy and emissions from parallel hybrid and conventional diesel buses fitted with selective catalytic reduction systems. Appl Energy 2015;159:433–41. https://doi.org/10.1016/j.apenergy.2015.09.007.
[12] Zhang S, Wu Y, Hu J, Huang R, Zhou Y, Bao X, et al. Can Euro V heavy-duty diesel engines, diesel hybrid and alternative fuel technologies mitigate NOX emissions? New evidence from on-road tests of buses in China. Appl Energy 2014;132:118–26. https://doi.org/10.1016/j.apenergy.2014.07.008.
[13] Luján JoséM, García A, Monsalve-Serrano J, Martínez-Boggio S. Effectiveness of hybrid powertrains to reduce the fuel consumption and NOx emissions of a Euro 6d-temp diesel engine under real-life driving conditions. Energy Convers Manag 2019;199:111987. https://doi.org/10.1016/j.enconman.2019.111987.
[14] Chang H, Li J, Chen X, Ma L, Yang S, Schwank JW, et al. Effect of Sn on MnO x-CeO 2 catalyst for SCR of NO x by ammonia: Enhancement of activity and remarkable resistance to SO 2. Catal Commun 2012;27:54–7. https://doi.org/10.1016/j.catcom.2012.06.022.
[15] Hao Z, Jiao Y, Shi Q, Zhang H, Zhan S. Improvement of NH 3 -SCR performance and SO 2 resistance over Sn modified CeMoO x electrospun fibers at low temperature. Catal Today 2019;327:37–46. https://doi.org/10.1016/j.cattod.2018.07.037.
[16] Damma D, Ettireddy P, Reddy B, Smirniotis P. A review of low temperature NH 3 -SCR for removal of NO x. Catalysts 2019;9(4):349. https://doi.org/10.3390/catal9040349.
[17] Wang TJ. Effects of insulation on exhaust temperature and subsequent SCR efficiency of a heavy-duty diesel engine. J Mech Sci Technol 2019;33(2):923–9. https://doi.org/10.1007/s12206-019-0149-9.
[18] Jiang J, Li D. Theoretical analysis and experimental confirmation of exhaust temperature control for diesel vehicle NOx emissions reduction. Appl Energy 2016;174:232–44. https://doi.org/10.1016/j.apenergy.2016.04.096.

[19] Hamedi MR, Doustdar O, Tsolakis A, Hartland J. Thermal energy storage system for efficient diesel exhaust aftertreatment at low temperatures. Appl Energy 2019; 235:874–87. https://doi.org/10.1016/j.apenergy.2018.11.008.

[20] Y. Okada, H. Hirabayashi, S. Sato, H. Inoue, Study on improvement of nox reduction performance at low temperature using urea reforming technology in urea SCR system, in: SAE Tech. Pap., SAE International, 2019. https://doi.org/10.4271/2019-01-0317.

[21] Rink M, Eigenberger G, Nieken U. Heat-integrated exhaust purification for natural gas engines. Chem-Ing-Tech 2013;85(5):656–63. https://doi.org/10.1002/cite.201200162.

[22] Rink M, Eigenberger G, Nieken U. Comparison of two different heat-integrated exhaust purification devices for monovalent CNG engines. Top Catal 2013;56(1-8): 421–6. https://doi.org/10.1007/s11244-013-9990-8.

[23] Sharp C, Webb CC, Yoon S, Carter M, Henry C, Low AU, et al. Heavy-Duty On-Highway TC Diesel Engine - Comparison of Advanced Technology Approaches. SAE Int J Engines 2017;10(2017):1722–35. https://doi.org/10.4271/2017-01-0956.

[24] Culbertson D, Khair M, Zhang S, Tan J, Spooler J. The Study of Exhaust Heating to Improve SCR Cold Start Performance. SAE Int J Engines 2015;8(3):1187–95. https://doi.org/10.4271/2015-01-1027.

[25] Massaguer A, Pujol T, Comamala M, Massaguer E. Feasibility study on a vehicular thermoelectric generator coupled to an exhaust gas heater to improve aftertreatment's efficiency in cold-starts. Appl Therm Eng 2020;167:114702. https://doi.org/10.1016/j.applthermaleng.2019.114702.

[26] Comamala M, Massaguer A, Massaguer E, Pujol T. Validation of a fuel economy prediction method based on thermoelectric energy recovery for mid-size vehicles. Appl Therm Eng 2019;153:768–78. https://doi.org/10.1016/j.applthermaleng.2019.03.004.

[27] Massaguer A, Massaguer E, Comamala M, Pujol T, González JR, Cardenas MD, et al. A method to assess the fuel economy of automotive thermoelectric generators. Appl Energy 2018;222:42–58. https://doi.org/10.1016/j.apenergy.2018.03.169.

[28] Massaguer E, Massaguer A, Pujol T, Comamala M, Montoro L, Gonzalez JR. Fuel economy analysis under a WLTP cycle on a mid-size vehicle equipped with a thermoelectric energy recovery system. Energy 2019;179:306–14. https://doi.org/10.1016/j.energy.2019.05.004.

[29] Gao J, Tian G, Sorniotti A, Karci AE, Di Palo R. Review of thermal management of catalytic converters to decrease engine emissions during cold start and warm up. Appl Therm Eng 2019;147:177–87. https://doi.org/10.1016/j.applthermaleng.2018.10.037.

[30] Moffat RJ. Describing the uncertainties in experimental results. Exp Therm Fluid Sci 1988;1(1):3–17. https://doi.org/10.1016/0894-1777(88)90043-X.

[31] Coleman HW, Steele WG. Experimentation, validation, and uncertainty analysis for engineers. Fourth edition 2018. https://doi.org/10.1002/9781119417989.

[32] Hewawasam LS, Jayasena AS, Afnan MMM, Ranasinghe RACP, Wijewardane MA. Waste heat recovery from thermo-electric generators (TEGs). In: Energy Reports. Elsevier Ltd; 2020. p. 474–9. https://doi.org/10.1016/j.egyr.2019.11.105.

[33] Massaguer E, Massaguer A, Montoro L, Gonzalez JR. Development and validation of a new TRNSYS type for the simulation of thermoelectric generators. Appl Energy 2014;134:65–74. https://doi.org/10.1016/j.apenergy.2014.08.010.

[34] Suter C, Jovanovic ZR, Steinfeld A. A 1kWe thermoelectric stack for geothermal power generation - Modeling and geometrical optimization. Appl Energy 2012;99: 379–85. https://doi.org/10.1016/j.apenergy.2012.05.033.

[35] M. Chrysostomou, N. Christofides, A review on solar thermal waste heat energy recovery using thermoelectric generators, 2016.

[36] Massaguer E, Massaguer A, Montoro L, Gonzalez JR. Modeling analysis of longitudinal thermoelectric energy harvester in low temperature waste heat recovery applications. Appl Energy 2015;140:184–95. https://doi.org/10.1016/j.apenergy.2014.12.005.

[37] Massaguer E, Massaguer A, Pujol T, Gonzalez JR, Montoro L. Modelling and analysis of longitudinal thermoelectric energy harvesters considering series-parallel interconnection effect. Energy 2017;129:59–69. https://doi.org/10.1016/j.energy.2017.04.061.

[38] Lan S, Yang Z, Stobart R, Chen R. Prediction of the fuel economy potential for a skutterudite thermoelectric generator in light-duty vehicle applications. Appl Energy 2018;231:68–79. https://doi.org/10.1016/j.apenergy.2018.09.087.

[39] Shen ZG, Tian LL, Liu X. Automotive exhaust thermoelectric generators: Current status, challenges and future prospects. Energy Convers Manag 2019;195:1138–73. https://doi.org/10.1016/j.enconman.2019.05.087.

[40] Massaguer A, Massaguer E, Comamala M, Pujol T, Montoro L, Cardenas MD, et al. Transient behavior under a normalized driving cycle of an automotive thermoelectric generator. Appl Energy 2017;206:1282–96. https://doi.org/10.1016/j.apenergy.2017.10.015.

[41] Comamala M, Pujol T, Cózar IR, Massaguer E, Massaguer A. Power and Fuel Economy of a Radial Automotive Thermoelectric Generator: Experimental and Numerical Studies. Energies 2018;11(10):2720. https://doi.org/10.3390/en11102720.

[42] Comamala M, Cózar IR, Massaguer A, Massaguer E, Pujol T. Effects of design parameters on fuel economy and output power in an automotive thermoelectric generator. Energies 2018;11:3274. https://doi.org/10.3390/en11123274.

[43] Fernández-Yañez P, Armas O, Capetillo A, Martínez-Martínez S. Thermal analysis of a thermoelectric generator for light-duty diesel engines. Appl Energy 2018;226: 690–702. https://doi.org/10.1016/j.apenergy.2018.05.114.

[44] Marvão A, Coelho PJ, Rodrigues HC. Optimization of a thermoelectric generator for heavy-duty vehicles. Energy Convers Manag 2019;179:178–91. https://doi.org/10.1016/j.enconman.2018.10.045.

[45] Di Battista D, Di Bartolomeo M, Villante C, Cipollone R. On the limiting factors of the waste heat recovery via ORC-based power units for on-the-road transportation sector. Energy Convers Manag 2018;155:68–77. https://doi.org/10.1016/j.enconman.2017.10.091.

[46] Vittorini D, Cipollone R, Carapellucci R. Enhanced performances of ORC-based units for low grade waste heat recovery via evaporator layout optimization. Energy Convers Manag 2019;197:111874. https://doi.org/10.1016/j.enconman.2019.111874.

[47] Villani M, Tribioli L. Comparison of different layouts for the integration of an organic Rankine cycle unit in electrified powertrains of heavy duty Diesel trucks. Energy Convers Manag 2019;187:248–61. https://doi.org/10.1016/j.enconman.2019.02.078.

[48] Gtisoft, GT-SUITE Overview | Gamma Technologies, (2017). https://www.gtisoft.com/gt-suite/gt-suite-overview/.

[49] Hasanpour Omam S. Exhaust waste energy recovery using Otto-ATEG-Stirling engine combined cycle. Appl Therm Eng 2021;183:116210. https://doi.org/10.1016/j.applthermaleng.2020.116210.

[50] Cózar IR, Pujol T, Lehocky M. Numerical analysis of the effects of electrical and thermal configurations of thermoelectric modules in large-scale thermoelectric generators. Appl Energy 2018;229:264–80. https://doi.org/10.1016/j.apenergy.2018.07.116.

[51] Hussain QE, Brigham DR, Maranville CW. Thermoelectric exhaust heat recovery for hybrid vehicles, in. SAE Tech Pap 2009;2(1):1132–42. https://doi.org/10.4271/2009-01-1327.

[52] Zienna N. A Model to Evaluate The Potential Benefits of a Thermoelectric Generator in Reducing CO2 Emisssions. Proc Eur GT Conf 2017.

[53] Maciá-Barber E. Thermoelectric Mater: Adv Appl 2015. https://doi.org/10.4032/9789814463539.

[54] Sandoz-Rosado EJ, Weinstein SJ, Stevens RJ. On the Thomson effect in thermoelectric power devices. Int J Therm Sci 2013;66:1–7. https://doi.org/10.1016/j.ijthermalsci.2012.10.018.

[55] I. Frank P, D. David P, B. Theodore L, L. Adrenne S, Fundamentals of Heat and Mass Transfer: Sixth Edition, 2019.